Structure and surface tension of interfaces between demixing liquids: model calculations using integral equations

2001 J. Phys.: Condens. Matter 13 4769

(http://iopscience.iop.org/0953-8984/13/21/309)

INSTITUTE OF PHYSICS PUBLISHING JOURNAL OF PHYSICS: CONDENSED MATTER

J. Phys.: Condens. Matter **13** (2001) 4769–4787 www.iop.org/Journals/cm PII: S0953-8984(01)21341-1

Structure and surface tension of interfaces between demixing liquids: model calculations using integral equations

Stanislav Iatsevitch and Frank Forstmann

Institut für Theoretische Physik, Freie Universität Berlin, Arnimallee 14, 14195 Berlin, Germany

Received 25 January 2001, in final form 9 April 2001

Abstract

A method for studying the structure and thermodynamic properties of interfaces between coexisting fluid phases has been developed recently. The density functional approach employs correlation functions calculated from reference hypernetted-chain integral equations. We report here results for liquid–liquid interfaces: the interface of a symmetrical binary Lennard-Jones mixture, a mixture of particles with different sizes and a polar–nonpolar liquid interface. Also model potentials for argon, CHF_3, C_6H_{12} and H_2O are tested with respect to surface properties.

1. Introduction

Fluid interfaces are systems that are currently of great interest. Many technical processes such as condensation and evaporation, wetting and drying, mixing and demixing, transport of solutes, formation of colloids and suspensions involve fluid interfaces. So there are many reasons to improve the understanding and the methods for analysis of interfaces between fluid phases. One path to more insight into the physics of fluid interfaces is that of elucidating the relations between the molecular interactions and the structure and thermodynamic interface properties. This paper is a contribution in such a direction and reports on statistical mechanics calculations of the interface properties of several model fluids, mixtures which separate and form fluid interfaces.

The statistical mechanics of inhomogeneous fluids is based here on density functional theory and the direct correlation function hierarchy. From the minimization of approximate density functionals the density profiles between fluid phases can be found (see [1–6] and for reviews see [7, 8]). Usually the term 'density functional theory' is used for approximations which introduce explicit functional density dependencies into expressions for the free energy. But the exact Euler equations for the minimum of the free energy contain the direct correlation functions $c_{\alpha\beta}(\boldsymbol{r}_1, \boldsymbol{r}_2)$. From density functional arguments one finds integral equations for $c_{\alpha\beta}(\boldsymbol{r}_1, \boldsymbol{r}_2)$ which are the second level of a hierarchy of equations for higher correlation functions. Closing the hierarchy of equations on this two-particle level leads to the integral equations (hypernetted chain (HNC) and reference HNC (RHNC) approximations, Percus–Yevick approximation, mean-spherical approximation etc) of the statistical mechanics of fluids.

0953-8984/01/214769+19$30.00

We have shown previously [6] that by calculating the two-particle correlations and employing these in the free energy, one can get very good results for the vapour–liquid interface of a Lennard-Jones fluid and for a Stockmayer fluid (Lennard-Jones plus dipole interaction). Here this method of calculation is tested by evaluating the structure and thermodynamic properties for liquid–liquid interfaces.

In the next section the essential steps of the calculation are explained and the necessary formulae are collected. For several details we will refer the reader to our previous papers [5,6]. Then the interface between symmetrical Lennard-Jones fluids is analysed (section 3) for which there are simulations available for comparison. For fluids with different diameters, results are given in section 4. In section 5 the LJ parametrization of the interaction of argon is tested with respect to the surface tension. Potential models for cyclohexane (section 6) and for the dipolar liquids CHF_3 and H_2O (section 7) are developed for the purpose of making calculations for a C_6H_{12}–water interface in section 8. Section 9 draws some conclusions.

2. The method for calculating the interface properties

The basic ideas of the density functional method for studying inhomogeneous fluids can be summarized as follows. The free energy of the system is constructed as a functional of the density distributions of the components and the equilibrium distributions are found by minimizing this functional. The nontrivial part is the construction of the 'excess free energy' $\mathcal{F}_{ex}$ which derives from the interactions of the particles forming the fluid. The roughest 'van der Waals approximation' replaces $\mathcal{F}_{ex}$ by the average potential energy neglecting all correlations. The exact $\mathcal{F}_{ex}$ can be written as a functional integral over correlation functions, either the total correlation functions $h_{\alpha\beta}(\boldsymbol{r}_1, \boldsymbol{r}_2) = g_{\alpha\beta}(\boldsymbol{r}_1, \boldsymbol{r}_2) - 1$ (with pair distribution function $g_{\alpha\beta}$) or the direct correlation functions $c_{\alpha\beta}(\boldsymbol{r}_1, \boldsymbol{r}_2)$. Neither the functions h or c nor their functional dependence on density distributions are known exactly for given interactions. Here several steps of approximation have to be taken in order to arrive finally at the thermodynamic properties of the system. We have developed a scheme of approximations which was shown to be successful for liquid–vapour interfaces [5, 6]. Here the reasoning and some of the formulae are collected which we later apply to liquid–liquid interfaces. The more detailed exposition in our previous papers also contains all the necessary references to the many authors who contributed to the density functional theory of liquids. Here we quote only the review book edited by D Henderson [9].

The evaluation procedure is based on the calculated direct correlation functions $c_{\alpha\beta}(\boldsymbol{r}_1, \boldsymbol{r}_2; [\rho])$. They are defined as second functional derivatives of the excess free energy $\mathcal{F}_{ex}$:

$$-\beta \frac{\delta^2 \mathcal{F}_{ex}[\rho]}{\delta\rho_\alpha(1)\,\delta\rho_\beta(2)} = \frac{\delta c_\alpha(1;[\rho])}{\delta\rho_\beta(2)} = c_{\alpha\beta}(1,2;[\rho]) \tag{1}$$

and fulfil two equations, the Ornstein–Zernike equation

$$h_{\alpha\beta}(1,2) = c_{\alpha\beta}(1,2) + \sum_\gamma \int \mathrm{d}3\; h_{\alpha\gamma}(1,3)\rho_\gamma(3)c_{\gamma\beta}(3,2) \tag{2}$$

and

$$h_{\alpha\beta}(1,2) + 1 = \exp\left[-\frac{1}{k_B T}u_{\alpha\beta}(1,2) + \sum_\gamma \int \mathrm{d}3\; h_{\alpha\gamma}(1,3)\rho_\gamma(3) \int_0^1 \mathrm{d}\lambda\; c_{\gamma\beta}(3,2;[\rho^\lambda])\right]. \tag{3}$$

In equation (3) the functional integral over a sequence of density distributions leads from the densities $\{\rho_\gamma(3)\}$ to the structured conditional densities $\{g_{\alpha\gamma}(1,3)\rho_\gamma(3)\}$ which the particles

of the different kinds γ show at position 3 when a particle of kind α with the potentials $u_{\alpha\gamma}(1, 3)$ sits at position 1. The arguments 1, 2 or 3 may include in addition to the particle position $\boldsymbol{r}$ internal variables like Euler angles θ, φ for dipole directions.

One form of the Euler equation that can be used to determine the density functions across a fluid boundary which minimize the free energy is the Lovett–Mou–Buff–Wertheim (LMBW) equation:

$$\nabla_1 \ln \rho_\alpha(1) = -\frac{1}{k_B T} \nabla_1 \Phi_\alpha(1) + \sum_\gamma \int \mathrm{d}2\, c_{\alpha\gamma}(1, 2; [\rho])\, \nabla_2 \rho_\gamma(2). \tag{4}$$

Here Φ_α is an external potential.

The equations (2), (3) and (4) are exact equations which are obtained from density functional derivatives of the free energy. They are not really a closed set because equation (3) for the two-particle correlations actually contains with $c_{\gamma\beta}(3, 2)$ near a particle α at position 1 three-particle correlations, for which a third level of equations exists in the hierarchy.

Standard practice closes these equations by using some approximations. We choose the RHNC approximation due to Lado [10, 11]. The HNC approximation replaces the integrals in equation (3) by those in equation (2) neglecting the functional dependence of $c_{\gamma\beta}(3, 2)$ on $[\rho]$. The RHNC approximation adds a correction $B_{\alpha\beta}(1, 2)$ in the exponent which is designed in order to get the results for hard-sphere systems exactly when the attractive part of the potential is switched off:

$$h_{\alpha\beta}(1, 2) + 1 = \exp\left[-\frac{1}{k_B T} u_{\alpha\beta}(1, 2) + h_{\alpha\beta}(1, 2) - c_{\alpha\beta}(1, 2) + B_{\alpha\beta}(1, 2)\right]. \tag{5}$$

$B_{\alpha\beta}(1, 2)$ is calculated from analytically available correlation functions for mixtures of hard spheres [12–17]. This RHNC approximation has proven to yield reliable bulk thermodynamic data, especially when the approximation is optimized by choosing the hard-core radii such that a measure of the thermodynamic inconsistency

$$\Delta^{\mathrm{RHNC}} = \frac{F}{V} + p - \sum_\alpha \rho_\alpha \mu_\alpha. \tag{6}$$

is minimized, in many cases made to vanish [5, 6, 18, 19]. When equations (2) and (5) are solved iteratively for a chosen temperature T and densities ρ_α, one can evaluate the pressure p and the chemical potentials μ_α. The extended formulae are given in [20] and for the reference hard-core mixture in [13] and [15]. For given T and concentration of one phase, one can determine the coexisting bulk phases in the case of demixing fluids.

The interface properties are calculated by solving equation (4) across the inhomogeneous interface region. In order to keep the numerical effort reasonable, we do not calculate the direct correlation functions in the inhomogeneous densities which are required in equation (4) directly from equations (2) and (5), but determine $c_{\alpha\beta}$ by interpolation between calculated functions for homogeneous fluids. We use the following steps of interpolation:

$$c_{\alpha\beta}(1, 2; [\rho]) = \frac{1}{2}\Big[c_{\alpha\beta}\big(|1 - 2|, \{\bar{\rho}_\gamma(\boldsymbol{r}_1)\}\big) + c_{\alpha\beta}\big(|1 - 2|, \{\bar{\rho}_\gamma(\boldsymbol{r}_2)\}\big)\Big]. \tag{7}$$

For a planar interface parallel to the x–y plane we take the weighted densities $\{\bar{\rho}_\alpha(1)\}$ as

$$\bar{\rho}_\alpha(z) = \int_{-\infty}^{+\infty} \mathrm{d}z'\; w_\alpha(z, z')\rho_\alpha(z'). \tag{8}$$

We choose

$$\bar{\rho}_\alpha(z) = \frac{1}{d_\alpha} \int_{z+s_\alpha-d_\alpha/2}^{z+s_\alpha+d_\alpha/2} \mathrm{d}z'\; \rho_\alpha(z'). \tag{9}$$

The weighting function $w_\alpha(z, z')$ has the form of a box around z with a width d_α and a shift s_α of its centre:

$$w_\alpha(z, z') = \begin{cases} 1/d_\alpha & z + s_\alpha - d_\alpha/2 \leqslant z' \leqslant z + s_\alpha + d_\alpha/2 \\ 0 & \text{otherwise.} \end{cases} \tag{10}$$

We have seen in [5] and [6] that as a result of the asymmetrical weighting due to the shift s_α, the iteration of the LMBW equation becomes stationary; that is, the position of the interface does not move at each iteration step. This means that we really have constructed an integro-differential equation whose solution is the interface density profile.

A second step of interpolation is used to get $c_{\alpha\beta}\big(|1-2|, \{\bar\rho_\gamma\}\big)$ for densities $\{\bar\rho_\gamma\}$ in the interface region from correlation functions calculated for homogeneous systems of compositions which border the compositions encountered in the interface, usually the co-existing phases and some low densities from the centre of the interface.

The interpolation yields correlation functions also for densities and concentrations in the interface region for which homogeneous systems would be unstable. The interpolation scheme has the additional advantage that the process of solving equation (4) iterates only on the densities and does not require recalculation of correlation functions from equations (2) and (5). It can be formally summarized as

$$c_{\alpha\beta}(1, 2; [\rho_\gamma]) = \frac{1}{2}\sum_k [\tau_k(z_1) + \tau_k(z_2)] c_{\alpha\beta}\big(|1-2|, \{\rho_\gamma^k\}\big). \tag{11}$$

The index k runs over all homogeneous phases where the $c_{\alpha\beta}$ have been calculated. The interpolation coefficients $\tau_k(z)$ depend on the weighted densities $\{\bar\rho_\gamma(z)\}$ and vary during iteration. More details can be found in [5, 6].

Equations (7), (9), (11) describe an approximate construction of direct correlation functions in regions of inhomogeneous densities. We have learned [6, 21–23] that approximating the direct correlation functions $c_{\alpha\beta}(1, 2)$ leads to safer, more robust and more successful procedures than approximations of the total correlation functions $h_{\alpha\beta}(1, 2)$. In our opinion the $c_{\alpha\beta}$ are simpler functions which change less with the thermodynamic parameters temperature, density and concentration. Therefore interpolation has a better chance. By this reasoning we also choose a formula for the surface tension which involves the $c_{\alpha\beta}$, the 'Triezenberg–Zwanzig formula' [6, 24–26]:

$$\beta\gamma = \frac{1}{4}\sum_{\alpha\beta}\int \mathrm{d}z_1\, \mathrm{d}\omega_1\, \frac{\partial\rho_\alpha(z_1\omega_1)}{\partial z_1}\int \mathrm{d}z_2\, \mathrm{d}\omega_2\, \frac{\partial\rho_\beta(z_2\omega_2)}{\partial z_2} \times \int \mathrm{d}\boldsymbol{R}_{12}\, R_{12}^2 c_{\alpha\beta}(R_{12}, z_1\omega_1, z_2\omega_2; \{\rho_\gamma(1)\}). \tag{12}$$

Here also the integration over the Euler angles $\omega = (\theta, \varphi)$ of the orientation of dipoles (sections 7, 8) is noted. When this method of calculation was used at liquid–vapour interfaces and the results compared with simulations, we found that in order to get really good results one has to observe in addition to the consistency related to equation (6) in the homogeneous phases another internal consistency requirement: the LMBW equation (4) itself predicts the coexisting phases as the limits on both sides of the interface from the integration of $(\mathrm{d}/\mathrm{d}z)\rho_\gamma(z)$, the solutions of equation (4). One side can be chosen but the other is a result of the calculation. Consistency of the entire procedure requires that these coexisting phases agree with those which had been determined from p and μ_α for the homogeneous phases. The parameters d_α and s_α of the weighting function $w_\alpha(z, z')$ in equation (10) are varied to adjust this consistency. Such slight variations of the interpolation of the direct correlation functions can lead to internal consistency. We always found that taking this additional trouble improved the results markedly.

The surface tension depends very much on the density differences across the interface. These are more reliably calculated by the bulk RHNC coexistence calculations.

This concludes the description of the various steps of our method for calculating the interface structure. We again refer the reader to our previous papers [5, 6] for further details, explicit formulae and more references, and also for the formulae for angle-dependent potentials, densities and correlation functions required for dipole interactions as treated in section 7 and section 8. Then the coordinate $1 = (\boldsymbol{r}_1, \omega_1)$, where $\omega_1 = (\theta_1, \varphi_1)$ gives the direction of the dipole of the particle at $\boldsymbol{r}_1$. The densities and correlation functions in the case of dipolar interactions are expanded in spherical harmonics. In the previous paper [6] we learned that a very short expansion yields very good thermodynamic data at coexistence.

3. The liquid–liquid interface of a symmetrical Lennard-Jones mixture

First the interface between two demixing Lennard-Jones liquids A and B is studied. As a test for the method we investigate a system which has also been studied in MD simulations by Toxvaerd and Stecki [27–29]. The system is symmetric with respect to A and B. The tendency for demixing is introduced by reducing the A–B attraction relative to A–A and B–B attraction:

$$u_{\alpha\beta}(1,2) = 4\varepsilon_{\alpha\beta}\left[\left(\frac{\sigma_{\alpha\beta}}{r_{12}}\right)^{12} - a_{\alpha\beta}\left(\frac{\sigma_{\alpha\beta}}{r_{12}}\right)^{6}\right] \tag{13}$$

$$\begin{aligned} &\varepsilon_{\mathrm{AA}} = \varepsilon_{\mathrm{BB}} = \varepsilon_{\mathrm{AB}} = \varepsilon \\ &\sigma_{\mathrm{AA}} = \sigma_{\mathrm{BB}} = \sigma_{\mathrm{AB}} = \sigma \\ &a_{\mathrm{AA}} = a_{\mathrm{BB}} = 1 \qquad a_{\mathrm{AB}} = 0.25. \end{aligned} \tag{14}$$

Also this potential can be represented by only two parameters by setting $\sigma' = \sigma a^{-1/6}$, $\varepsilon' = \varepsilon a^2$. These fluids can therefore be compared to simple Lennard-Jones fluids by corresponding-states arguments.

When the surface tension is derived from simulations, there is usually a problem with the long-range tail of the potential. When simulating the structure of the interface and evaluating the particle distributions, usually the potential is cut off at a certain distance, while for the surface tension, a 'long-tail correction' is added [30, 31]. Then the structure and the surface free energy are principally calculated with different potentials. Recently a simulation by Mecke *et al* [31] has included the long-tail correction also in the determination of the density profiles at a liquid–vapour interface (see [6]). For the liquid–liquid interface the simulation of Stecki and Toxvaerd [28] evaluates the surface tension with a cut-off Lennard-Jones potential. We want to compare our result with this simulation. Therefore the same Lennard-Jones interactions are used, equations (13), (14), cut off at $r_c = 2.5\sigma$ and shifted upwards by $|u_{\alpha\beta}(r_c)|$ to avoid a discontinuity:

$$\tilde{u}_{\alpha\beta}(r) = \begin{cases} u_{\alpha\beta}(r) - u_{\alpha\beta}(r_c) & r < r_c \\ 0 & r \geqslant r_c. \end{cases} \tag{15}$$

The other parameters for the test calculation are chosen from one of the systems simulated by Stecki and Toxvaerd (reference [28], line 7 of table 1). The temperature is $T^* = kT/\varepsilon = 1$, well below the liquid–gas critical temperature ($T_c^* = 1.31$ for the uncurtailed LJ potential [32]). The surface tension is very sensitive to the density and pressure of the system. We choose the density such that the calculated pressure is equal to the pressure in the simulated system $p^* = p\sigma^3/\varepsilon = 2.0417$ [28]. The bulk density is then $\rho^* = \rho\sigma^3 = 0.8186$. In a simulation the pressure is a constant throughout the whole simulation box and is therefore a safer parameter for equality of systems than the bulk density, which is reached only in small parts of the box.

Now all parameters are fixed, there is nothing left for fitting. The procedures outlined in section 2 are followed. The symmetry of the system simplifies the search for coexistence. For total density $\rho = \rho_A + \rho_B$ and concentration $c = \rho_B/\rho$ one gets

$$\begin{aligned} p(\rho, c) &= p(\rho, 1-c) \\ \mu_A(\rho, c) &= \mu_B(\rho, 1-c) \\ \mu_B(\rho, c) &= \mu_A(\rho, 1-c). \end{aligned} \tag{16}$$

Therefore the coexisting phases can be found by searching only in one phase for the concentration $\bar{c}$ with $\mu_A(\rho, \bar{c}) = \mu_B(\rho, \bar{c})$. Then the coexisting concentration is $\tilde{c} = 1 - \bar{c}$. For temperatures below the demixing critical point a solution $\bar{c} \neq 0.5$ is found, which has a lower free energy than the mixture with $\rho_A = \rho_B$ and $c = 0.5$.

In figure 1 the density profiles $\rho_A(z)$, $\rho_B(z)$ and the total density $\rho(z) = \rho_A(z) + \rho_B(z)$ are shown. In the interface the total density decreases because there weak A–B bonds are numerous and the cohesion is reduced. The shaded part represents the (negative) Gibbs adsorption $\Gamma = \Gamma_A + \Gamma_B = -0.76\sigma^{-2}$. The Gibbs adsorption is defined as

$$\Gamma = \int_{-\infty}^{+\infty} (\rho(z) - \rho_{bulk})\, \mathrm{d}z = \frac{1}{\sigma^2} \int_{-\infty}^{+\infty} (\rho^*(z) - \rho^*_{bulk})\, \mathrm{d}(z/\sigma). \tag{17}$$

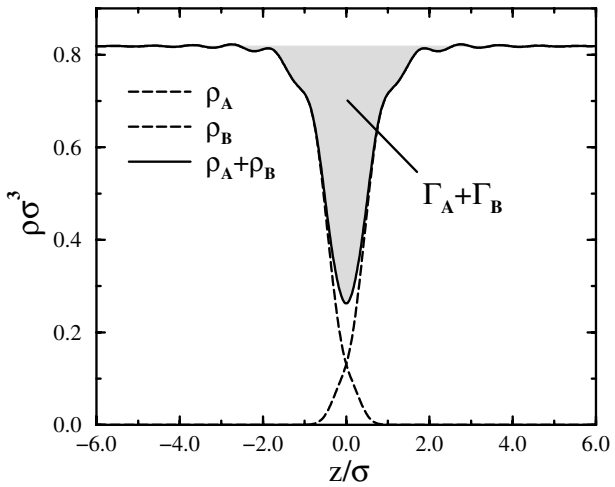

Figure 1. The density profiles at the interface between the A-rich and the B-rich phase. $T^* = k_B T/\varepsilon = 1$, $\rho^*_{bulk} = 0.8186$; the shaded area shows the Gibbs adsorption.

In the symmetric system, Γ does not depend on the Gibbs dividing surface.

The density oscillations near the interface indicate a layer structure. Also with other non-local density functionals such oscillations have been found at fluid interfaces [1,2,33] and they are also demonstrated in the simulations with comparable size and wavelength [27,28]. The examples plotted in the publications cited are for a stronger demixing tendency $a_{AB} = 0$ and there the oscillations have even larger amplitudes.

The evaluation of the interface tension by formula (12) yields $\gamma^* = \gamma\sigma^2/\varepsilon = 1.78$ which agrees with the MD simulation result $\gamma^* = 1.71$ [28] within 4%, within the accuracy of the simulation. We learn from this result that the integration of the LMBW equation (4) with approximations for the direct correlation functions developed in section 2 and optimized according to the recipes of section 2 is a reliable and robust method for studying fluid interfaces. Also for liquid–vapour surfaces the method worked successfully [6]. In a previous paper [5]

we did not curtail the potential. With the larger attraction more cohesion, higher density and a much larger tension, $\gamma^* = 4.66$, result. Other authors have found, too, that the 'long-tail correction' to simulation results can double the surface tension [30].

Next the temperature was increased at fixed bulk density $\rho^* = 0.8186$. The results are shown in figures 2–5. The density profiles in figure 2 get broader with a much smaller density drop in the middle of the interface. The oscillations in the density indicating a layer structure are only present at low temperatures. The 10%–90% width, the separation of the z-values between which $[\rho_B(z) - \rho_B(\text{right})]/[\rho_B(\text{left}) - \rho_B(\text{right})]$ varies from 0.1 to 0.9, is shown in figure 3. It increases at higher temperatures and should go to infinity at the demixing critical temperature. The absolute value of the Gibbs adsorption (figure 3) decreases with growing temperature, but rather slowly.

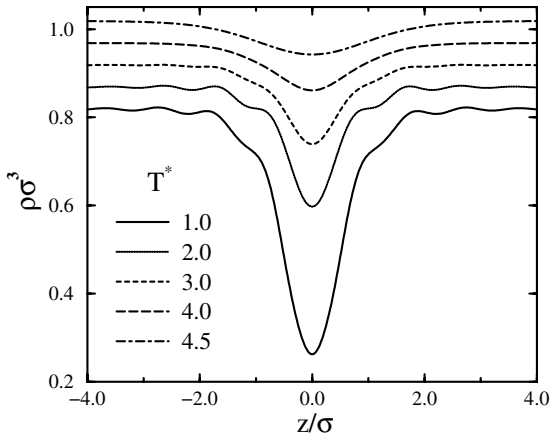

Figure 2. Temperature dependences of the total-density profiles.

The concentrations in figures 4 demonstrate the broadening of the interface but appear sharper than the density profiles. An interesting result is the fact that the concentration profiles do not show the oscillations which are seen in the density. This has also been found in simulations [27, 28] and in our calculations for the liquid–vapour interface [5].

The surface tension versus temperature at fixed bulk density goes through a maximum in figure 5. At a liquid–vapour surface it usually decreases monotonically because in equation (12) the density gradients and c decrease. This behaviour is seen in γ_{gl}, the contribution to γ from interactions between the same kinds of particle, A–A and B–B, in equation (12). In contrast, the part γ_{fr} from A–B interactions is increasing when increasing temperature mixes the particles near the interface more strongly and therefore increases the total energy of the system because of the weak A–B attraction. These two opposite trends form the maximum. A recent simulation result shows the same qualitative behaviour [34].

4. A Lennard-Jones mixture with different particle sizes

Another model studied is a Lennard-Jones mixture with different sizes. The results show different densities and concentrations in the A-rich and B-rich phases.

The model is defined by Lennard-Jones interactions, equation (13), with the parameters

$$\begin{aligned} &\varepsilon_{AA} = 1.0 \qquad \varepsilon_{BB} = 1.0 \qquad \varepsilon_{AB} = 0.5 \qquad a_{\alpha\beta} = 1.0 \\ &\sigma_{AA} = 1.0 \qquad \sigma_{BB} = 1.84 \qquad \sigma_{AB} = \tfrac{1}{2}(\sigma_{AA} + \sigma_{BB}) = 1.42. \end{aligned} \tag{18}$$

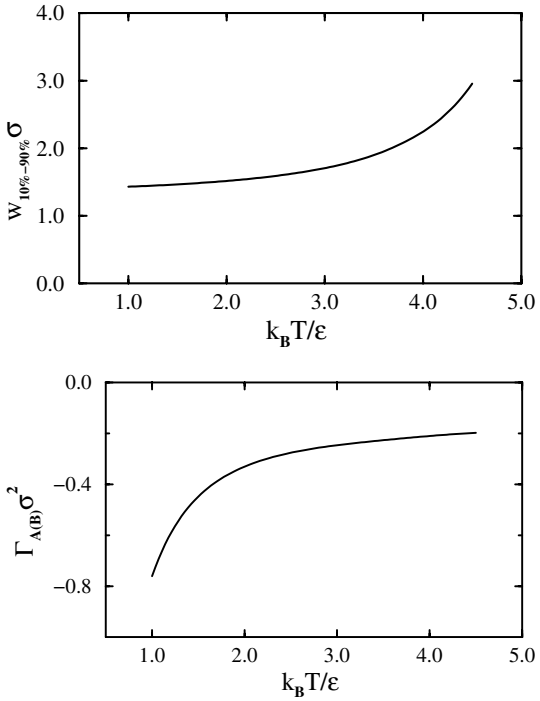

Figure 3. Temperature dependences of the 10%–90% width and the Gibbs adsorption.

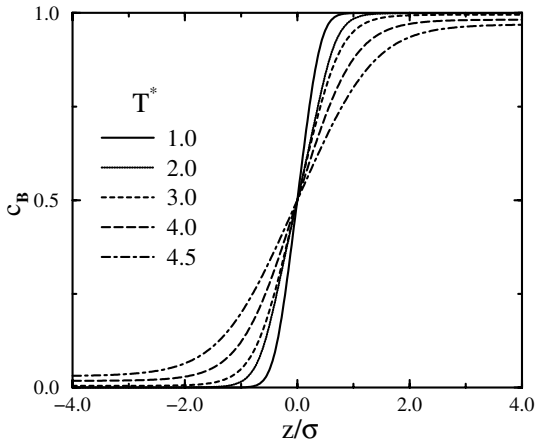

Figure 4. Concentrations of particles of type B across the interface.

In figure 6 we plot the densities $\rho^*_\alpha = \rho_\alpha \sigma^3_{\mathrm{AA}}$ and the packing fractions ξ, the fractions of particle volume over total volume:

$$\xi_\alpha = \frac{\pi}{6}\rho_\alpha \sigma^3_{\alpha\alpha}. \tag{19}$$

Both representations show strong layering on the side where the large particles B are in the majority. The packing fractions in the bulk are fairly equal because the pressure is constant throughout the system and $\varepsilon_{\mathrm{AA}} = \varepsilon_{\mathrm{BB}}$, but it drops in the interface where many weak A–B

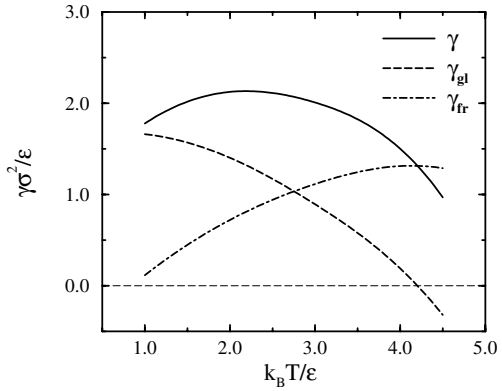

Figure 5. The temperature dependence of the surface tension γ at fixed density. γ is separated into the contribution from identical particles γ_{gl} and that from unequal particles γ_{fr}.

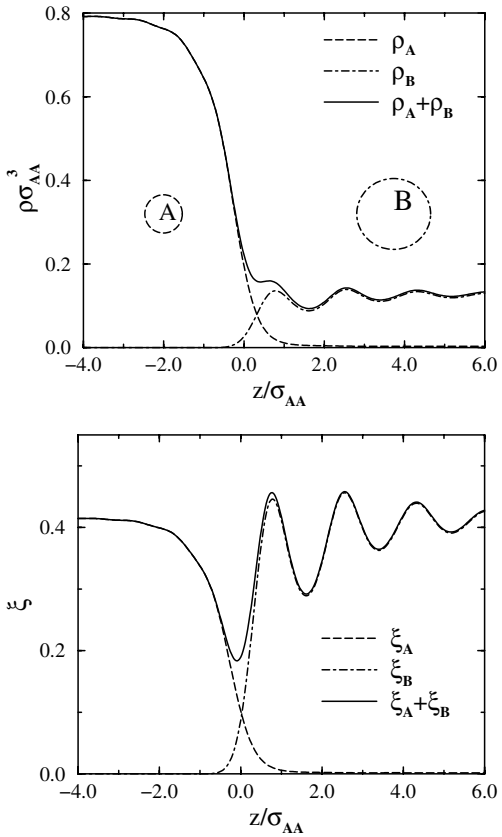

Figure 6. Densities and packing fractions $\xi_\alpha = \rho_\alpha \sigma_{\alpha\alpha}^3 \pi/6$ across the interface between LJ liquids of different particle sizes.

interactions play a role. The period of oscillation is close to the diameter of the majority particles, and also to that of the weak oscillations on the A-rich side. The surface tension in this system was calculated to be $\gamma^* = \gamma\sigma_{\mathrm{AA}}^2/\varepsilon_{\mathrm{AA}} = 0.94$.

Lennard-Jones mixtures have also been studied by means of simpler density functionals, using the mean-field approximation [35,36] or square gradient approximation [37,38], mainly with respect to wetting of the liquid–vapour interface. At liquid–liquid interfaces no density oscillations have been found by those methods.

5. The surface tension of argon

In this section different criteria for modelling argon by means of Lennard-Jones potentials are investigated. That the Lennard-Jones 6–12 potential is a useful *ansatz* has been proven for low-density rare gases [39]. Several gas properties can be calculated well with the same potential parameters—for instance the second virial coefficient, the viscosity and the heat conductivity. For argon, the fit to the virial coefficient yields

$$\text{from the virial coefficient:} \qquad \sigma = 3.405 \text{ Å} \qquad \varepsilon/k_B = 119.8 \text{ K}. \tag{20}$$

For liquid densities, coexistence and surface properties, it is possible that other parameters lead to better results. We have found [6] that correct coexistence densities are very important for yielding good surface tensions. We test in figure 7 how well the coexistence curve of argon is described by a Lennard-Jones coexistence line and which parameters fit the data best. We use an interpolation of a simulated coexistence curve for a Lennard-Jones system [32,40] which is given in reduced units, and rescale it with the parameters from a virial coefficient fit. In figure 7 the critical temperature comes out too high. From a rescaling of the simulated curve via a least-squares fit to the experimental data, one gets the following parameters:

$$\text{from the coexistence data:} \qquad \sigma = 3.389 \text{ Å} \qquad \varepsilon/k_B = 114.5 \text{ K}. \tag{21}$$

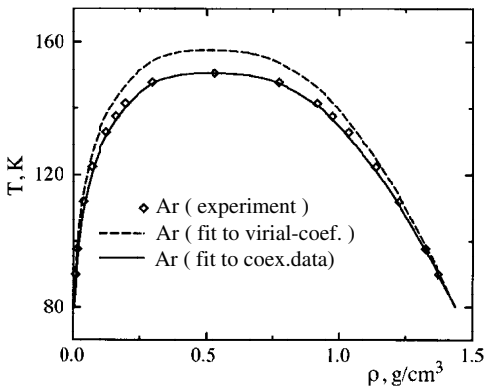

Figure 7. The coexistence curve for argon for different LJ potentials.

Next the surface tension is calculated for these two parameter sets along the lines of section 2: coexistence from RHNC equations (2), (5) and evaluation of p, μ; the surface structure from LMBW equation (4), with optimized approximations; then evaluation of γ from equation (12). Figure 8 shows the results. The coexistence fit improves the calculated values very much. The deviations from the experimental values are less than 10% in the temperature range studied, while the parameters derived from the virial coefficient lead to errors of 20% to 40%.

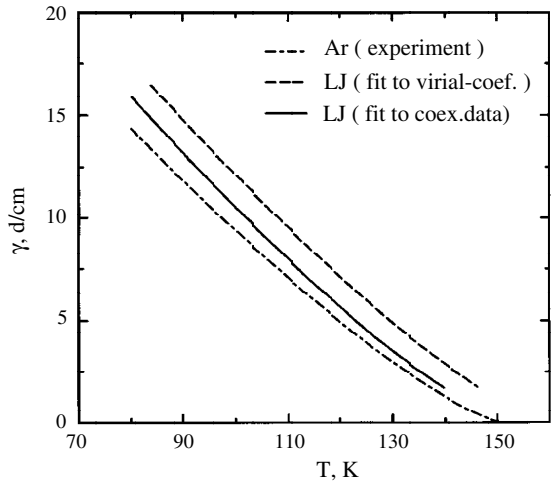

Figure 8. The surface tension of argon versus temperature.

6. A fit of a Lennard-Jones potential for cyclohexane to surface tension data

Surface and interface properties present more crucial tests for a potential model than bulk coexistence data. We have studied to what extent a Lennard-Jones potential works for cyclohexane C_6H_{12}. Measured coexistence data and surface tension data are taken, the LJ parameters are fitted to one property, the other is calculated and the deviations are tested. The fit to the coexistence curve with stress on the critical temperature and on the liquid densities at lower temperatures yields

$$\text{from the coexistence data:} \qquad \sigma = 5.333 \text{ Å} \qquad \varepsilon/k_B = 422.1 \text{ K}. \tag{22}$$

At $T_{exp} = 25\ ^\circ$C the coexistence liquid density is $\rho_{exp} = 0.7739$ g cm^{-3} and the surface tension is $\gamma = 24.38$ dyn cm^{-1}. The Lennard-Jones potential parameters ε and σ lead for $T = 25\ ^\circ$C to

$$\rho(\varepsilon, \sigma) = \rho_{exp} \tag{23}$$

$$\gamma(\varepsilon, \sigma) = \gamma_{exp}. \tag{24}$$

The solution can be found from the principle of corresponding states, which relates the thermodynamic properties of all fluids with the same form ϕ of the potential $u(r) = \varepsilon\phi(r/\sigma)$ with one energy parameter ε and one parameter σ for the length scale [39,41]. The temperature T, pressure p, density ρ and surface tension γ have to be expressed in reduced units:

$$T^* = Tk_B/\varepsilon \qquad p^* = p\sigma^3/\varepsilon \qquad \rho^* = \rho\sigma^3 \qquad \gamma^* = \gamma\sigma^2/\varepsilon. \tag{25}$$

For instance the equation of state $f(p^*, T^*, \rho^*) = 0$ is valid for all fluids with the same potential form [39]. Also the temperature dependence of the surface tension $\gamma^*(T^*)$ has a universal character [41]. The liquid density $\rho^*(T^*)$ at coexistence and $\gamma^*(T^*)$ were calculated for a liquid–vapour surface of a Lennard-Jones system [6]. Therefore we transform equations (23), (24) as follows:

$$\rho^*(\tilde{T}^*) = \rho_{exp}\sigma^3 \tag{26}$$

$$\frac{1}{\tilde{T}^*}\gamma^*(\tilde{T}^*) = \gamma_{exp}\sigma^2/(k_B T_{exp}) \tag{27}$$

with $\tilde{T}^* = k_B T_{exp}/\varepsilon$. We now consider the left-hand sides as functions of ε, the right-hand sides as functions of σ, plot both sides parametrically in figure 9 and take ε and σ from the point where the curves cut each other and equations (26), (27) are fulfilled:

$$\text{from the surface tension:} \qquad \sigma = 5.344 \text{ Å} \qquad \varepsilon/k_B = 430.3 \text{ K}. \tag{28}$$

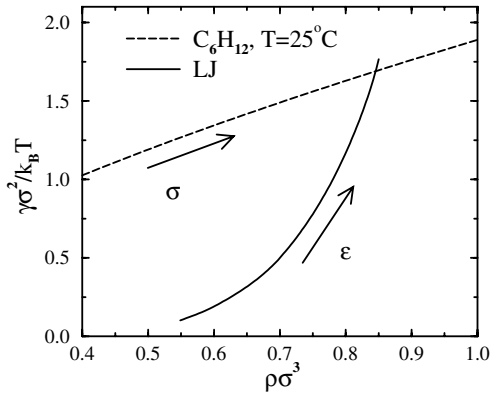

Figure 9. Determination of σ and ϵ of the LJ potential for C_6H_{12}.

For both parameter sets (22) and (28), we show the coexistence curves in figure 10 (produced by scaling an interpolation of simulated results as in figure 7) and the temperature dependence of the surface tension γ evaluated via LMBW equation (4) and equation (12) in figure 11. The deviations are systematic, but not large. When one reduces the critical temperature by 2%, the surface tension is reduced by 5% to 10%.

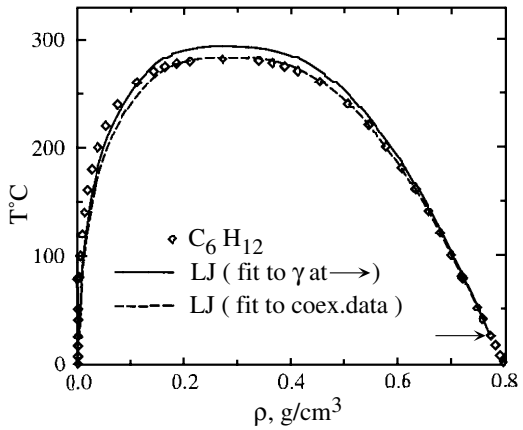

Figure 10. The coexistence curve for C_6H_{12} for different LJ potentials.

In general it can be concluded that the Lennard-Jones parametrization of the cyclohexane interaction is reliable even as regards interface properties. We expect such parametrization to be even better for more spherical molecules like CH_4, CCl_4, CF_4. There have been proposals for Lennard-Jones parametrizations for *n*-alkanes [42]. With an approximate density functional it was shown that parameters derived from coexistence data and from the surface tension deviate more as the chains of the alkanes become longer. With an additional parameter for the potential range, the situation can be improved [42].

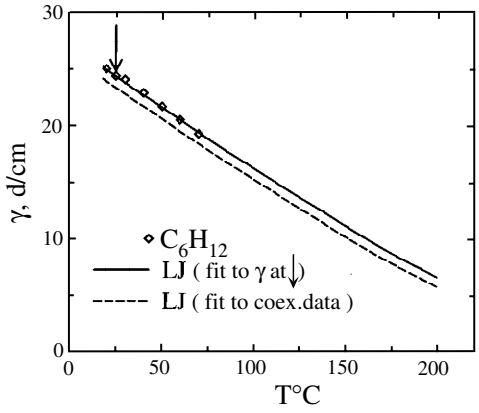

Figure 11. The surface tension of C_6H_{12} versus temperature.

7. The Stockmayer fluid, a model for dipolar solvents

The Stockmayer fluid, a system with spherical Lennard-Jones interactions and dipoles at the centres of the particles, is a model for solvents composed of polar molecules. We study here to what extent this model can approximate properties of trifluoromethane (CHF_3) and of water. CHF_3 is a small nearly spherical molecule with a dipole moment of $1.62\ \mathrm{D} = 5.39 \times 10^{-30}\ \mathrm{C\,m}$ (D $\equiv$ Debye unit). Water molecules are of similar size and also the dipole moment of $1.82\ \mathrm{D} = 6.06 \times 10^{-30}\ \mathrm{C\,m}$ is close, but the anisotropy of the interaction between water molecules is much lager than for CHF_3 and therefore more difficulties in describing it using a Stockmayer potential can be expected.

A procedure analogous to that of the previous section is followed and for each fluid a Lennard-Jones potential as well as a Stockmayer potential are found which reproduce the experimental liquid density and surface tension at a given temperature:

$$\begin{aligned} \rho(\varepsilon, \sigma, \mu) &= \rho_{exp} \\ \gamma(\varepsilon, \sigma, \mu) &= \gamma_{exp}. \end{aligned} \tag{29}$$

ρ_{exp} is the coexistence density of the liquid and γ_{exp} is the measured surface tension. We will determine model parameters from equation (29) and then calculate other properties to see how adequately the Stockmayer potential models the interactions and to understand the contribution from the dipole interaction. The dipole moment μ is set equal to that measured for the gas molecules or to zero for comparison with simple Lennard-Jones potentials. As in the previous section, corresponding-states arguments are used [39, 41]:

$$\begin{aligned} \rho^*(T^*, \mu_T^{*\,2}) &= \rho_{exp}\sigma^3 \\ \frac{\gamma^*(T^*, \mu_T^{*\,2})}{T^*} &= \frac{\gamma_{exp}\sigma^2}{k_B T_{exp}} \end{aligned} \tag{30}$$

with $\mu_T^{*\,2} = \mu_{exp}^2/(k_B T_{exp}\sigma^3)$. The corresponding-states rules mean for the Stockmayer fluid that e.g. $\gamma^*(T^*, \mu_T^{*\,2})$ has the same dependence on T^* for all values of ε and σ, provided that $\mu_T^{*\,2}$ has a fixed value. We therefore choose some values, $\mu_T^{*\,2} = 1, 1.5, 2$, and solve the equations (30) graphically in figure 12.

For CHF_3 the experimental values are $\rho_{exp} = 1.3098\ \mathrm{g\,cm^{-3}}$ and $\gamma_{exp} = 15\ \mathrm{dyn\,cm^{-1}}$ at $T_{exp} = 199.85\ \mathrm{K}$. The right-hand sides of equations (30) are plotted in figure 12. The

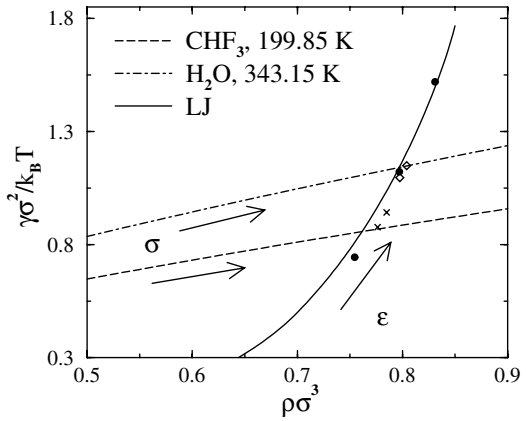

Figure 12. Determination of σ and ϵ of the LJ potential for CHF_3 and H_2O. The points are for the Stockmayer model: ${\mu_T^*}^2 = 1$ (•), ${\mu_T^*}^2 = 1.5$ (×), ${\mu_T^*}^2 = 2$ (◇).

parameter along the line is σ. For water, $\rho_{exp} = 0.977$ g cm^{-3}, $\gamma_{exp} = 64.27$ dyn cm^{-1} for $T_{exp} = 343.15$ K are taken. The integral equation result for the Lennard-Jones fluid is the continuous line (as in figure 9), where ε and therefore T^* are varied. The Stockmayer potential results for ${\mu_T^*}^2 = 1$, 1.5 and 2 and for several ε-values are very close to the line for pure Lennard-Jones potentials. This result means that a certain density of the liquid leads to a well defined surface tension determined by the Lennard-Jones interaction, no matter what the dipole strength is. The analysis of the nonspherical contribution to γ in section 8 leads to the same idea: the dipole interaction may change the density and cohesion, but only in this way can it influence γ.

Because ${\mu_T^*}^2 = \mu^2/(k_B T\sigma^3)$ depends on the diameter resulting from the points at which the lines in figure 12 cross, a quick iteration is necessary for different values of ${\mu_T^*}^2$ in order to find μ_T^* which relates to the experimental dipole moment. The resulting parametrizations for the two systems CHF_3 and H_2O are given in table 1. Also the pure Lennard-Jones potential parameters are shown which solve equations (30) with $\mu = 0$.

Table 1. LJ and Stockmayer potential parameters for CHF_3 and H_2O with the calculated critical temperatures and the deviations from the experimental values.

		${\mu_T^*}^2$	ϵ/k_B (K)	σ (Å)	T_c (K)	$T_{c,exp}$ (K)	δT_c (%)
CHF_3	LJ	0	213.87	3.971	280.8	299.3	6.2
CHF_3	Stockmayer	1.54	194.13	3.994	293.4	299.3	2.0
H_2O	LJ	0	426.6	2.900	560.1	647.1	13.4
H_2O	Stockmayer	2.09	328.2	2.908	531.7	647.1	17.8

The critical temperature of the model systems can be derived from the simulation result $T_c^* = T_c k_B/\varepsilon = 1.313$ (for a pure Lennard-Jones system [32]). Also for Stockmayer models there is a parametrized summary of several MD simulations by van Leeuwen [43, 44]:

$$T_c^* = 1.313 + 0.2999\mu^{*2} - 0.2837\ln(\mu^{*2} + 1). \tag{31}$$

Here $\mu^{*2} = \mu^2/(\varepsilon\sigma^3) = {\mu_T^*}^2 k_B T/\varepsilon$. The models underestimate the critical temperature of CHF_3 which is measured as $T_{c,exp} = 299.3$ K, but introducing the dipole interaction increases it and it comes close, within 2%. The cohesion due to the dipoles is not simply added to the Lennard-Jones interaction, but ε must be taken smaller in order to approach γ and the

coexistence density at lower temperatures. We conclude that the Stockmayer model is rather good for CHF_3.

For water the outcome is not as successful. Adding the dipole interaction makes the critical temperature worse. Obviously the Stockmayer model misses some of the essential interactions in water, the hydrogen bridge bonds, which are responsible for the high experimental $T_c = 647.1$ K.

There is another problem with the Stockmayer model for water. $\mu_T^{*\,2} = 2.09$ in table 1 represents a dipole moment $\mu = 1.53$ D. If μ is increased to 1.82 D and $\mu_T^{*\,2}$ to 2.87 (at 343.15 K) at a water density of $\rho^* = 0.804$, the model is unstable with respect to a ferroelectric phase transition (see e.g. [45]). From a certain dipole strength upwards, the region where the Stockmayer model shows coexistence is limited to higher temperatures with smaller liquid densities.

In a paper by van Leeuwen [44], the parameters of the Stockmayer potential for 63 organic and inorganic fluids have been determined from fits to liquid–gas coexistence data, also for some molecules containing nitrogen, which have large dipole moments like $\mu^{*2} = \mu^2/\varepsilon\sigma^3 = 4.54$ for acrylonitrile or $\mu^{*2} = 8.05$ for acetonitrile. If the latter is transformed to units of kT at room temperature, $\mu_T^{*\,2} = 4.8$. Such a Stockmayer model at liquid densities is well within the ferroelectric regime and cannot be used to model acetonitrile. Most of the substances modelled in [44] are in the moderate regime $\mu^{*2} < 2$ and are far enough from the ordering transition.

8. A polar–nonpolar liquid interface

We have studied in section 6 the Lennard-Jones potential for cyclohexane and in section 7 the Stockmayer potential fitted to data for water. With these models we now make calculations for an interface between cyclohexane and water as an example of an interface with a dipolar component, as found in many technically important systems [39]. The interaction between cyclohexane and water is assumed to be a Lennard-Jones one with the diameter σ the sum of the two radii:

$$\sigma(C_6H_{12}\text{–}H_2O) = (\sigma(C_6H_{12}) + \sigma(H_2O))/2. \tag{32}$$

For determining $\varepsilon_{AB}(C_6H_{12}\text{–}H_2O)$ we take into account the degree of demixing and the interface tension but we cannot fit the experimental values perfectly with this single parameter. From [46] (by extrapolation) at 70 °C and $p = 760$ Torr one can derive the solubilities 0.3% H_2O in C_6H_{12} and 0.005% C_6H_{12} in H_2O with $\gamma = 49.09$ dyn cm^{-1} [47]. On decreasing ε_{AB} in the model interaction, the degree of demixing and the interface tension are increased.

First the water model without a dipole from section 7, table 1, is taken and $\varepsilon_{AB}/k_B = 214.2$ K chosen, which is just half of the Lorentz–Berthelot suggestion [48] of the geometric mean value $(\varepsilon_{AA}\varepsilon_{BB})^{1/2}$. With these model parameters there is still 6.6% water in C_6H_{12} while the large C_6H_{12} molecules have withdrawn from the water to leave a residual concentration of 0.000 04% (concentration $c_1 = \rho_1/(\rho_1 + \rho_2)$). Like in figure 13 for the Stockmayer potential, strong oscillations are also found here, i.e. layering on the side of the large C_6H_{12} molecules. The interface tension is $\gamma = 66$ dyn cm^{-1}, larger than measured. The approximation scheme for the direct correlation functions and its optimization (section 2) could not be carried out to complete consistency. The LMBW equation (4) led to a density of C_6H_{12} 5% larger than the RHNC coexistence calculation. This higher density is one reason for the larger surface tension.

Secondly the Stockmayer model for water from section 7 is used with the same H_2O–C_6H_{12} interaction (table 2). On introducing the water dipoles, the H_2O content in C_6H_{12} is slightly reduced to 5.7% and the C_6H_{12} content in water becomes a bit larger, 0.000 056%. The

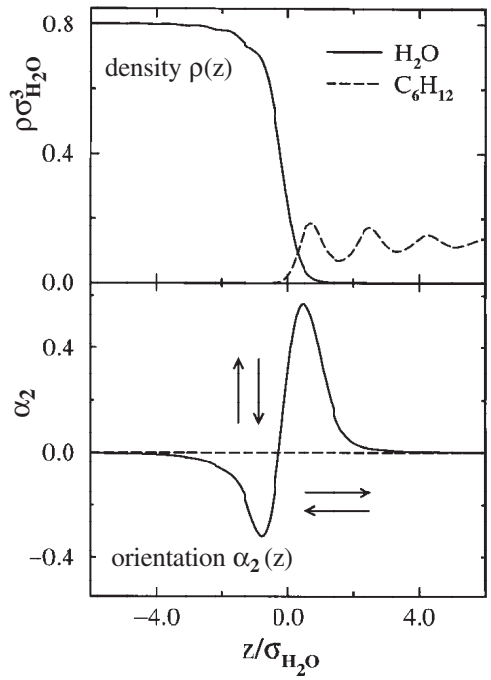

Figure 13. Densities and dipole orientation at the water–cyclohexane interface. $T = 70\ ^\circ$C; the Stockmayer–LJ model.

Table 2. Potential parameters for a water–cyclohexane mixture with the LJ and the Stockmayer models for water.

Components	$\mu_T^{*\,2}$	ϵ/k_B (K)	σ (Å)
H_2O (LJ)	0	426.6	2.900
H_2O (Stockmayer)	2.09	328.2	2.908
C_6H_{12}	0	430.3	5.344
C_6H_{12}–H_2O	0	214.2	4.122

move is in the right direction but too small. In figure 13 the density profiles are shown with even more pronounced layers on the cyclohexane side than without dipoles. Also the gradient on the water side is steeper. The result is a larger surface tension: $\gamma = 77$ dyn cm^{-1}, 18% above the measured value. In the lower panel of figure 13 the information about the dipole orientation is given. The angle-dependent density is expanded:

$$\rho(z, \Theta) = \rho(z) \sum_{\ell} \alpha_\ell(z) P_\ell(\cos\Theta). \tag{33}$$

As for the liquid–gas surface in [6], at the liquid–liquid interface the dipoles are found normal to the surface (positive values of α_2) on the side of low dipole density and parallel to the surface plane on the high-density side.

We discussed in [6] why the different extremal values of α_2 mean essentially the same degree of orientation. For perfect normal orientation $\alpha_2 = 5/2$, so with the calculated maximal value of $\alpha_{2,max} = 0.57$ we can speak of a degree of normal orientation $\alpha_{2,max}/(5/2) = 0.228$, while perfect parallel orientation yields $\alpha_2 = -5/4$ and the calculated degree of parallel orientation $\alpha_{2,min}/(-5/4) = 0.256$ on the side of high dipole density. As at the liquid–vapour

surface, we understand the dipole orientation from image force considerations: the low-density dipoles are in front of a medium of large polarizability with image charges of opposite sign. Then the normal orientation is the low-energy position. The dipoles on the high-density side are in a highly polarizable system in front of a half-space of low dielectric constant. This leads to image charges of the same sign where the parallel position has lower energy. The degree of orientation at the liquid–liquid interface is much larger than at a liquid–vapour surface of a Stockmayer fluid (see [6]).

We can compare only to simulations, which use much more complicated potentials: a water/benzene interface was investigated in Monte Carlo simulations by Linse [49] while molecular dynamics was used for water/octane by Zhang *et al* [50] and for water/ethylene chloride by Benjamin [51–53]. We did not find simulations of a Stockmayer–Lennard-Jones interface. Model dipoles were represented by opposite charges on two-centre Lennard-Jones molecules like CO [54, 55]. The mean-field density functional calculations concentrated on the liquid–vapour interface of polar–nonpolar mixtures [4, 56, 57]. All simulations found essentially the same orientation. If the resolution is not sophisticated enough, the simulations see only the parallel orientation of the many dipoles on the high-density side and not the normal orientation of the few.

Because dipole forces contribute to the average cohesion one may ask whether the dipole forces alone can lead to demixing. We have therefore studied the system with $\varepsilon_{AB} = [\varepsilon(H_2O)\varepsilon(C_6H_{12})]^{1/2}$ according to the Lorentz–Berthelot suggestion. Here the Lennard-Jones potentials do not lead to demixing, but also the addition of dipole forces of strength $\mu^{*2} = 2.09$ did not lead to separated phases. Previously a separation of hard spheres from hard spheres with dipoles was predicted for $\mu_T^{*2} = \mu^2/\sigma^3 kT = 2.5$ and $\rho^* > 0.6$ [58]. For Stockmayer models, simulations by de Leeuw *et al* [59, 60] showed a dipole-driven demixing for large $\mu^{*2} = \mu^2/\sigma^3\varepsilon > 3.15$ at $T^* = Tk_B/\varepsilon = 1.15$ and $\rho^* = \rho\sigma^3 = 0.822$.

In the system studied here the demixing is caused by an A–B isotropic Lennard-Jones interaction that is weak compared to the A–A and B–B LJ interaction. The H_2O–H_2O attraction is very close to that within C_6H_{12}. Therefore the strong asymmetry of the concentrations in the coexisting phases is due to the different sizes of the particles. The small water molecules dissolve better within the phase of large cyclohexane molecules than vice versa. The dipolar interactions contribute very little to this picture.

9. Conclusions

Interfaces between demixing liquids were investigated by density functional methods employing calculated correlation functions. In a previous paper [6] we developed this scheme of calculation, especially a certain sequence of approximations. Parameters in these approximations were optimized by the requirement of internal thermodynamic consistency. Then it was shown how well the procedure worked at liquid–vapour interfaces. Here the method is tested at interfaces between two liquids.

An exact comparison with an MD simulation is possible for a symmetrical Lennard-Jones mixture (section 3). The potentials are curtailed in the same way as in the simulations. The calculated surface tension agrees with the evaluation from the simulation within the accuracy of the simulation. This result proves the reliability of the method also in the case of a liquid–liquid interface. As a second example a LJ mixture with very different sizes of the particles was chosen (section 4). Strong density oscillations, i.e. a layering, on the side of the larger particles are the prominent result.

Next for the case of argon we tested whether the LJ parametrization of the interaction yields good results also at the surface (section 5). The surface tension comes out closer than

10% to the measured result when the LJ parameters are determined from coexistence data, while the standard fit to the virial coefficient is less satisfactory. That coexistence data and the surface tension correspond well is also found for cyclohexane in section 6. In section 7 we studied fluids with dipole interactions. At the liquid–vapour surface the dipole interaction contributes to the cohesion and therefore increases the liquid density, but for the given density the evaluation of the surface tension shows very little contribution from the dipole forces. For a molecule which is nearly spherical with a dipole, like CHF_3, the Stockmayer potential can be parametrized to yield the coexistence data and the surface tension well, while for H_2O the critical temperature comes out too low by about 15% when the surface tension at lower temperatures is used for the parameter fit.

Finally the interface calculation was evaluated for an interface between a polar and a nonpolar liquid (section 8). The orientation of the dipoles at this interface is qualitatively the same as at the liquid–vapour surface, but the degree of order is much higher. The results demonstrate that the method for investigating fluid interfaces works under several very different conditions, that the approximations are robust and that the results are excellent when they can be compared to simulations which use the same potentials.

Acknowledgment

The financial support of the Deutsche Forschungsgemeinschaft is gratefully acknowledged.

References

[1] Evans R, Henderson J R, Hoyle D C, Parry A O and Sabeur Z A 1993 *Mol. Phys.* **80** 755
[2] Evans R, Leote de Carvalho R J F, Henderson J R and Hoyle D C 1994 *J. Chem. Phys.* **100** 591
[3] Frodl P and Dietrich S 1993 *Phys. Rev.* E **48** 3741
[4] Teixeira P I C, Almeida B S, Telo da Gama M M, Rueda J A and Rubio R G 1992 *J. Phys. Chem.* **96** 8488
[5] Iatsevitch S and Forstmann F 1997 *J. Chem. Phys.* **107** 6925
[6] Iatsevitch S and Forstmann F 2000 *Mol. Phys.* **98** 1309
[7] Evans R 1990 *Liquids at Interfaces (Les Houches Summer School Lectures)* vol 2, ed J Charvolin, J F Joanny and J Zinn-Justin (Amsterdam: Elsevier) p 1
[8] Evans R 1992 *Fundamentals of Inhomogeneous Fluids* ed D Henderson (New York: Dekker) pp 85–175
[9] Henderson D (ed) 1992 *Fundamentals of Inhomogeneous Fluids* (New York: Dekker)
[10] Lado F 1964 *Phys. Rev.* **135** A1013
[11] Lado F 1976 *Mol. Phys.* **31** 1117
[12] Lebowitz J L 1964 *Phys. Rev.* A **4** 895
[13] Lebowitz J L and Rowlinson J S 1964 *J. Chem. Phys.* **41** 133
[14] Lebowitz J L, Helfand E and Praestgaard E 1965 *J. Chem. Phys.* **43** 774
[15] Mansoori G A, Carnahan N F, Starling K E and Leland T W Jr 1971 *J. Chem. Phys.* **54** 1523
[16] Grundke E W and Henderson D 1972 *Mol. Phys.* **24** 269
[17] Lee L L and Levesque D 1973 *Mol. Phys.* **26** 1351
[18] Lado F, Foiles S M and Ashcroft N W 1983 *Phys. Rev.* A **28** 2374
[19] Lomba E 1989 *Mol. Phys.* **68** 87
[20] Chen X S, Forstmann F and Kasch M 1991 *J. Chem. Phys.* **95** 2832
[21] Alts T, Nielaba P, D'Aguanno B and Forstmann F 1987 *Chem. Phys.* **111** 223
[22] Kasch M and Forstmann F 1993 *J. Chem. Phys.* **99** 3037
[23] Kasch M and Forstmann F 1994 *Ber. Bunsenges. Phys. Chem.* **98** 497
[24] Rowlinson J S and Widom B 1982 *Molecular Theory of Capillarity* (Oxford: Clarendon)
[25] Triezenberg D G and Zwanzig R 1972 *Phys. Rev. Lett.* **28** 1183
[26] Lovett R, Dehaven P W, Vieceli J J Jr and Buff F P 1973 *J. Chem. Phys.* **58** 1880
[27] Toxvaerd S and Stecki J 1995 *J. Chem. Phys.* **102** 7163
[28] Stecki J and Toxvaerd S 1995 *J. Chem. Phys.* **103** 4352
[29] Stecki J and Toxvaerd S 1995 *J. Chem. Phys.* **103** 9763
[30] Holcomb C D, Clancy P and Zollweg J A 1993 *Mol. Phys.* **78** 437

[31] Mecke M, Winkelmann J and Fischer J 1997 *J. Chem. Phys.* **107** 9264
[32] Smit B 1992 *J. Chem. Phys.* **96** 8639
[33] Henderson J R and Sabeur Z A 1992 *J. Chem. Phys.* **97** 6750
[34] Diaz-Herrera E 2000 private communication
[35] Tarazona P, Telo da Gama M M and Evans R 1983 *Mol. Phys.* **49** 283
[36] Tarazona P, Telo da Gama M M and Evans R 1983 *Mol. Phys.* **49** 301
[37] Telo da Gama M M and Evans R 1983 *Mol. Phys.* **48** 229
[38] Telo da Gama M M and Evans R 1983 *Mol. Phys.* **48** 251
[39] Rowlinson J S 1959 *Liquids and Liquid Mixtures* (London: Butterworth)
[40] Lotfi A, Vrabec J and Fischer J 1992 *Mol. Phys.* **76** 1319
[41] Ono S and Kondo S 1960 *Handbuch der Physik* ed S Flügge (Berlin: Springer)
[42] Penfold R, Abbas S and Nordholm S 1996 *Fluid Phase Equil.* **120** 39
[43] van Leeuwen M E 1994 *Mol. Phys.* **82** 383
[44] van Leeuwen M E 1994 *Fluid Phase Equil.* **99** 1
[45] Klapp S and Forstmann F 1997 *J. Chem. Phys.* **106** 9742
[46] Bartels J *et al* (ed) 1956 *Landolt–Börnstein New Series* Group II, vol 2a (Berlin: Springer)
[47] Lax E and Synowietz C (ed) 1967 *D'Ans-Lax, Taschenbuch für Chemiker und Physiker* vol 1 (Berlin: Springer)
[48] Hansen J-P and McDonald I R 1986 *Theory of Simple Liquids* 2nd edn (London: Academic)
[49] Linse P 1987 *J. Chem. Phys.* **86** 4177
[50] Zhang Y, Feller S, Brooks B R and Pastor R W 1995 *J. Chem. Phys.* **103** 10 252
[51] Benjamin I 1992 *J. Chem. Phys.* **97** 1432
[52] Benjamin I 1993 *Science* **261** 1558
[53] Schweighofer K J and Benjamin I 1995 *J. Electroanal. Chem.* **391** 1
[54] Benjamin I 1991 *J. Phys. Chem.* **95** 6675
[55] Benjamin I 1992 *J. Chem. Phys.* **96** 577
[56] Luengo G, Aracil J, Rubio R and Diaz Peña M 1988 *J. Phys. Chem.* **92** 228
[57] Aracil J, Luengo G, Almeida B S, Telo da Gama M M, Rubio R G and Diaz Peña M 1989 *J. Phys. Chem.* **93** 3210
[58] Chen X S and Forstmann F 1992 *Mol. Phys.* **76** 1203
[59] de Leeuw S W, Williams C P and Smit B 1988 *Mol. Phys.* **65** 1269
[60] de Leeuw S W, Smit B and Williams C P 1990 *J. Chem. Phys.* **93** 2704